2005

Kinetic Desorption and Sorption of U(VI) during Reactive Transport in a Contaminated Hanford Sediment

Nikolla P. Qafoku
Pacific Northwest National Laboratory, nik.qafoku@pnl.gov

John M. Zachara
Pacific Northwest National Laboratory, john.zachara@pnl.gov

Chongxuan Liu
Pacific Northwest National Laboratory, chongxuan.liu@pnl.gov

Paul Gassman
Pacific Northwest National Laboratory, paul.gassman@pnl.gov

Odeta Qafoku
Pacific Northwest National Laboratory

See next page for additional authors

Environ. Sci. Technol. **2005**, *39,* 3157−3165

Kinetic Desorption and Sorption of U(VI) during Reactive Transport in a Contaminated Hanford Sediment

NIKOLLA P. QAFOKU,* JOHN M. ZACHARA, CHONGXUAN LIU, PAUL L. GASSMAN, ODETA S. QAFOKU, AND STEVEN C. SMITH

Pacific Northwest National Laboratory, P.O. Box 999, MSIN: K3-61, Richland, Washington 99301

Column experiments were conducted to investigate U(VI) desorption and sorption kinetics in a sand-textured, U(VI)-contaminated (22.7 μmol kg^{-1}) capillary fringe sediment from the U.S. Department of Energy (DOE) Hanford site. Saturated column experiments were performed under mildly alkaline conditions representative of the Hanford site where uranyl−carbonate and calcium−uranyl−carbonate complexes dominate aqueous speciation. A U(VI)-free solution was used to study contaminant U(VI) desorption in columns where different flow rates were applied. Sorbed, contaminant U(VI) was partially labile (11.8%), and extended leaching times and water volumes were required for complete desorption of the labile fraction. Uranium-(VI) sorption was studied after the desorption of labile, contaminant U(VI) using different U(VI) concentrations in the leaching solution. Strong kinetic effects were observed for both U(VI) sorption and desorption, with half-life ranging from 8.5 to 48.5 h for sorption and from 39.3 to 150 h for desorption. Although U(VI) is semi-mobile in mildly alkaline, subsurface environments, we observed substantial U(VI) adsorption, significant retardation during transport, and atypical breakthrough curves with extended tailing. A distributed rate model was applied to describe the effluent data and to allow comparisons between the desorption rate of contaminant U(VI) with the rate of short-term U(VI) sorption. Desorption was the slower process. We speculate that the kinetic behavior results from transport or chemical phenomena within the phyllosilicate-dominated fine fraction present in the sediment. Our results suggest that U(VI) release and transport in the vadose zone and aquifer system from which the sediment was obtained are kinetically controlled.

Introduction

Hexavalent uranium [U(VI)] is a groundwater contaminant at numerous sites in the United States (*1*). Groundwater plumes of U(VI) with a high probability of migrating and discharging to nearby rivers exist at several U.S. Department of Energy (DOE) sites where nuclear materials were handled and processed. A typical example is the Hanford 300 Area U(VI) groundwater plume (*2*). The plume underlies a 7−10 m vadose zone that was contaminated by the passage of U(VI)-containing waste fluids discharged to infiltration basins. This particular U(VI) plume at Hanford has not dissipated as rapidly as anticipated, and many questions exist regarding the geochemical and hydrologic causes for this behavior.

U(VI) is generally considered a mobile or semi-mobile contaminant at circumneutral pH (*3*). This is especially so at Hanford where mildly alkaline conditions promote subsurface migration (*4*). Carbonate forms stable neutral (*5*, *6*) or anionic (*7*, *8*) aqueous complexes with U(VI) in such environments increasing its overall mobility (*9*−*12*). Aqueous uranyl carbonate species, however, adsorb to varying degrees on hydroxylated mineral surfaces (*12*). The retardation extent of U(VI) under mildly alkaline conditions is therefore controlled by competition between aqueous and surface complexation.

The Hanford 300A U(VI) groundwater plume is in hydraulic connection with the Columbia River, a water resource of tremendous economic and cultural significance in the northwestern United States. Hydrologic coupling between the vadose zone, aquifer, and river system create seasonal hydrologic and geochemical transients that have complex effects on U(VI) groundwater composition. U(VI) desorption from contaminated sediments may occur during the relatively wet season when small amounts of drainage pass through the vadose zone. But what makes this system especially dynamic is that short-term changes in groundwater flow occur in response to changes in the Columbia River stage (*2*). During high river stage conditions, the groundwater table rises into the lower vadose zone, and U(VI) may be desorbed or sorbed depending on the specific aqueous and sediment concentrations of U(VI). Therefore, sediments of the lower vadose zone may serve as both a source and a sink for U(VI) in this complex aquifer system.

The kinetics of U(VI) desorption and adsorption, if slow relative to porewater velocity, could exert an important influence on the long-term evolution and dissipation of a U(VI) groundwater plume such as that at Hanford. U(VI) adsorption to hematite demonstrated a rapid initial phase of 30 min and a longer phase extending to hundreds of hours (*13*). Similar trends were observed for other minerals and sediments (*14*−*16*). At faster pore water velocities, U(VI) adsorption in a goethite column was far from equilibrium (*17*), and U(VI) adsorption during unsaturated transport in a silt loam (56% silt) and sand (98% sand) textured Hanford sediment was affected by rate-limited mass transfer (*18*, *19*). Slow U(VI) adsorption has been attributed to intraparticle diffusion, redistribution between sites with different reactivity, and/or surface precipitation. The literature, however, offers few insights on the rates of U(VI) sorption and desorption in contaminated vadose and saturated zones.

We investigated U(VI) desorption and sorption in a contaminated capillary fringe sediment using water-saturated laboratory columns. A mildly alkaline, carbonate solution similar in composition to the Hanford groundwater was used as an electrolyte. Strong kinetic effects were observed for both U(VI) desorption and sorption. A distributed rate model was applied to describe the effluent data and to allow comparisons between the kinetics of desorption of contaminant U(VI) that had been in contact with the sediment for 30 yr with the kinetics of short-term U(VI) adsorption. The laboratory results suggest that U(VI) release and transport in the field, are likely to be kinetically controlled.

Materials and Methods

Sediment and Mineralogical Analyses. The vadose zone sediment was collected in the South Process Pond of the 300

* Corresponding author phone: (509)375-4364; fax: (509)375-6954; e-mail: nik.qafoku@pnl.gov.

10.1021/es048462q CCC: $30.25
Published on Web 03/18/2005

TABLE 1. Composition of the SGW

analyte	concentration ($\times 10^{-4}$ mol L^{-1})
Na	15.3
Ca	5.97
Mg	5.29
K	4.30
DIC[a] ($[CO_3]_{TOT}$)	10.45
HCO_3 (calcd)[b]	10.33
CO_3 (calcd)[b]	0.11
SO_4	9.81
Br	6.23
NO_3	5.71
ionic strength	59.3
P_{CO_2}	$10^{-3.5}$ atm
pH	8.05

[a] DIC stands for dissolved inorganic carbon. [b] Speciation performed with MINTEQA2.

Area of the Hanford Site, WA, at 5.5 m depth below the current ground surface. It was slightly contaminated by the passage of U(VI) containing waste fluids over the period 1941−1973. The sediment was a Pleistocene age, near capillary-fringe material that overlaid a U(VI) groundwater plume containing U(VI) concentrations that range from ~0.042 to 1.05 μmol L^{-1} (*2*). Groundwater elevations at this location may vary by 1 m or more in response to Columbia River stage (*2*). We conducted particle size analysis of the <2 mm fraction of the sediment (*20*) and determined extractable Fe_{OX} and Fe_{DCB} with the ammonium oxalate and dithionite−citrate−bicarbonate methods, respectively (*21*−*23*).

Mineralogical analyses were performed on the clay fraction (<2 μm) and a mixture of silt and clay (hereafter called the fine fraction) that was isolated by sedimentation. The concentrated suspensions (3 g L^{-1}) of clays and fines were preferentially oriented on porous ceramic tiles; these were then saturated with either 1 mol L^{-1} KCl or MgCl and washed free of excess salts with DI water. The Mg-saturated materials were solvated with a solution of 20% glycerol. X-ray diffraction (XRD) measurements were performed at 25 °C and on the K-saturated samples after heating to 110, 300, and 550 °C for 4 h. The diffraction measurements were obtained with a Phillips X'Pert X-ray diffractometer operating in step scan mode, using Cu Kα radiation and a graphite monochromometer. Diffractograms were collected from 2 to 32° 2Θ for the 25 °C samples and from 2 to 16° 2Θ for the heated ones.

Column Electrolyte. A synthetic groundwater (SGW) with a pH of 8.05 (±0.04) and a total inorganic C ($[CO_3]_{TOT}$) concentration of 1.05×10^{-3} mol L^{-1} was used in all experiments (Table 1). Appropriate amounts of a 37.47 μmol L^{-1} $UO_2(NO_3)_2$ solution were used to prepare SGW solutions with different U(VI) concentrations (0, 0.35, 3.79, and 4.05 μmol L^{-1}). These electrolytes were continuously bubbled with air for at least 1 week before use, and they were stored in plastic bottles. Thermodynamic aqueous speciation and saturation index calculations were performed for these electrolytes using the MINTEQ2A computer program (*24*, *25*) with the database presented in Table SI-1 in the Supporting Information.

Column Experiments. The column methodology has been described elsewhere (*26*, *27*). For this study, six PVC columns (3.2 × 14.5 cm) were packed uniformly with the Hanford sediment. Column packing was performed in ~10 g increments that were then tamped by hand with a plastic dowel. Porous plates (0.25 cm thick and 10 μm pore diameter) were used at the top and bottom of each column to distribute the electrolyte and to collect fines (that were found to be minimal) at the column outlet. A high-performance liquid chromatography pump was used to control water flows to values that were similar to those observed in the Hanford 300 Area aquifer (up to 10 m d^{-1}). The physical properties of the columns and transport parameters are summarized in Table 2. The stop-flow (SF) technique (*28*) was frequently used to evaluate whether the transport process was at equilibrium.

Chemical Analyses of Column Effluents. A kinetic phosphorescence analyzer (model KPA-11, Chemchek Instruments) with an operational detection limit of 0.001 μmol L^{-1} was used to measure U(VI) concentrations in the effluents. A Br combination ion selective electrode (Accumet) was used to measure aqueous Br concentrations. Frequent pH measurements and some cation analyses (Ca, Mg, K, Na, Ba, Ni, Sr, Zn, and Cu) were performed in the effluent solutions.

Transport Parameters from Tracer Breakthrough Curves. The CXTFIT code was used to calculate transport parameters based on the Br breakthrough curves (BTC) (Figure SI-1 in the Supporting Information) (*29*, *30*). The experimental water flux was calculated as the average flow rate divided by the area of the column (Table 2). Mean pore water velocity (V) was calculated as the experimental water flux divided by the volumetric water content (θ), and the equilibrium adsorption model was used to calculate D (dispersion coefficient) and R (retardation coefficient). This model assumes that the column is at physical equilibrium. In several columns, we fitted the two-region, physical nonequilibrium model to the Br BTC data using R as a known parameter and D, β (the mobile water fraction), and ω (the mobile−immobile region exchange term) as unknown parameters (*31*). The results indicated that all water was mobile and that physical nonequilibrium played no significant role in Br transport. The dispersivity values ($\lambda = D/V$) were within the range of typical values observed in packed laboratory columns (λ < 2 cm) (*32*), and the values of the Peclet number ($Pe = L/\lambda$, where L is the column length) varied between 9 and 51 (Table 2).

Modeling. A 1-D, distributed rate coefficient model (*33*) was used to describe the column data. First-order rate coefficients for a hypothetical assemblage of reaction site groups were fitted according to a γ-distribution statistical model. The reaction sites within each group were assumed to exhibit the same kinetic behavior. No explicit assumption was made as to the cause of the kinetic behavior. A single value of distribution coefficient (K_d) (mL g^{-1}) was assumed for all sorption sites in a given model calculation. The change in U(VI) concentration with time in the aqueous and solid phase were described by eqs 1 and 2:

$$\theta\frac{\partial C}{\partial t} = \theta D\frac{\partial^2 C}{\partial x^2} - \theta V\frac{\partial C}{\partial x} - \sum_{i=1}^{N}\alpha_i\rho_b[f_i K_d C - S_i] \quad (1)$$

$$\frac{\partial S_i}{\partial t} = \alpha_i(f_i K_d C - S_i) \quad (2)$$

where θ is the volumetric water content (length^3 length^{-3}), C is the aqueous concentration (mass length^{-3}), D is the hydrodymanic dispersion coefficient (length^2 time^{-1}), V is the average pore water velocity (length time^{-1}), ρ_b is the bulk density (mass length^{-3}), and the subscript i is used for each specific site group having a site fraction of f_i, a rate coefficient of α_i (T^{-1}), and a sorbed concentration of S_i (mass sorbed/mass of sediment). The distribution of the first-order rate coefficients for the site assemblage was assumed to follow the gamma probability distribution (*33*):

$$P(\alpha) = \frac{\beta^{-\eta}\alpha^{\eta-1}}{\Gamma(\eta)}\exp\left(-\frac{\alpha}{\beta}\right) \quad (3)$$

where β is the scale parameter (T^{-1}), η is the shape parameter,

TABLE 2. Selected Physical Properties in Each Column

	column					
	1	2	3	4	5	6
pore volume[b] (cm^3)	46.4	49.6	49.0	46.7	46.3	47.7
water content[b] ($cm^3\ cm^{-3}$)	0.40	0.42	0.42	0.40	0.40	0.41
residence time[b] (h)	1.09	9.52	10.2	1.10	9.90	1.08
bulk density[b] ($g\ cm^{-3}$)	1.65	1.66	1.64	1.69	1.65	1.69
flow rate[a] ($cm^3\ min^{-1}$)	0.701 [0.040] (303)	0.087 [0.010] (886)	0.080 [0.003] (286)	0.710 [0.034] (316)	0.078 [0.006] (617)	0.735 [0.032] (355)
water flux ($cm\ min^{-1}$)	0.0883	0.0108	0.0099	0.0882	0.0097	0.0913
pore water velocity ($cm\ d^{-1}$)	319	36.6	34.1	317	35.2	321
dispersion coefficient ($cm^2\ d^{-1}$)	145	55.6	29.1	320	9.97	306
dispersivity (cm)	0.45	1.52	0.85	1.00	0.28	0.95
Peclet number	32	9	17	14	51	15

[a] The average flow rate was calculated from experimental measurements (the standard deviation is given in squared brackets, and the number of experimental measurements is given in parentheses). [b] Pore volume, water content, residence time, and bulk density were calculated based on the amount of sediments added in each column and the mass of water used to saturate the columns.

and $\Gamma(\eta)$ is the γ-function. From eq 3, the following expression was derived to describe f_i with a first-order kinetic rate constant of α_i:

$$f_i(\alpha_i) = \int_{\alpha_i}^{\alpha_i + \Delta\alpha_i} \frac{\beta^{-\eta}\alpha^{\eta-1}}{\Gamma(\eta)} \exp\left(-\frac{\alpha}{\beta}\right) d\alpha \qquad (4)$$

We determined V and θ by direct measurement. D was determined by fitting the Br BTC in each column, while K_d, β, and η were determined simultaneously by fitting the U(VI) BTC. The magnitude of the fitted K_d was determined by the residual, labile, sorbed U(VI) before and the U(VI) effluent concentrations after the SF events. The K_d values may be correlated with the rate constants to some extent. However, sensitivity calculations implied that the correlation was small because large variation in rate parameters had minimal effect on the fitting of the stop flow concentration spikes while K_d did. The interdependence between K_d values and β and η was therefore minimal. The model was also used to calculate the average rate constant for the adsorption and desorption in each experiment.

Results and Discussion

Sediment Characterization. Particle size analysis showed that 93% of the <2 mm particles were sand, 5% were silt, and the remaining 2% were clay. Extractable Fe_{OX} and Fe_{DCB} were 48 and 77 μmol g^{-1}, respectively. The total U in the sediment as determined by X-ray fluorescence was <22.7 μmol kg^{-1}. A 1:2 sediment to water suspension yielded a pH of 8.14. The "indigenous" U(VI) labile fraction mobilized after 3 weeks of treatment with a 1.44×10^{-2} mol L^{-1} $NaHCO_3$ and 2.8×10^{-3} mol L^{-1} Na_2CO_3 solution with a pH of 9.45 (*34*) was 2.68 μmol kg^{-1} or 11.8% of the total. Previous mineralogical analyses of Hanford sediments have shown that the overall mineralogy is dominated by quartz, with lesser amounts of feldspars and hornblende (*4*). The clay and fine fractions extracted from this sediment exhibited similar mineralogy (Figures SI-2 and SI-3 in the Supporting Information). The approximate mass percentages of the most abundant minerals in the clay fraction were smectite (41%), muscovite (19%), vermiculite (19%), and chlorite (15%). Phyllosilicates were less abundant in the fine fraction because it contained larger amounts of quartz and feldspars. The sediment contained little or no calcite (<0.01% inorganic carbon).

Aqueous Speciation of the SGW. The computed U(VI) aqueous speciation in the SGW was dominated by calcium−uranyl−carbonate complexes (Table SI-2 in the Supporting Information). The distribution of species was slightly dependent on $U(VI)_{aq}$ concentration. The SGW was undersaturated with respect to calcite and any of the uranyl solids present in our thermodynamic database. However, because the crystal chemistry of U(VI) is complex and the solubility of many U(VI) solids are not well-known, the precipitation of U(VI), although unlikely, cannot be excluded as a potential retardation mechanism in these studies.

Quantifying the Desorption Process. To investigate the time dependency of U(VI) desorption kinetics from the contaminated sediment, two column experiments with different flow regimes (FRT of 1.09 and 9.52 h in columns 1 and 2, respectively) were performed. Both columns were initially leached for more than 90 PV with the same SGW solution ($[CO_3]_{TOT} = 1.05 \times 10^{-3}$ mol L^{-1}) that simulated the site pore/groundwater composition. The desorption of U(VI) from the contaminated sediment was a slow process and decreased with time during leaching (Figure 1). Over 100 PV of SGW was required to desorb the small labile U(VI) fraction that existed at an initial concentration of 2.68 μmol kg^{-1} (0.64 ppm). The effluent U(VI) concentration reached a maximum of 0.12 and 0.17 μmol L^{-1} in the first 5 PV in the fast- and slow-flow columns, respectively, and decreased thereafter. The regulatory limit for groundwater U at this location is 0.126 μmol L^{-1} or 30 ppb.

The SF technique was used to investigate whether equilibrium conditions were established and to study the direction and extent of time-dependent reaction. The $U(VI)_{aq}$ concentration sharply increased during the SF events in both columns, although the magnitude of change in the slow column decreased as leaching progressed. The total amount of U(VI) released in the slow column was 1.85 μmol kg^{-1}, which was approximately 69% of the U(VI) labile fraction of 2.68 μmol kg^{-1}.

The γ-distribution model has been successfully used to describe time-dependent processes in soils and sediments (*33*, *35*−*42*). The use of this numeric model is consistent with two alternative conceptual physicochemical models: (i) a chemically controlled system containing a large number of binding site groups that each exhibits comparable U(VI) sorptivity (e.g., K_d) but different desorption (or sorption) rates or (ii) a mass transfer controlled system containing a wide distribution of pore or diffusional path lengths (*35*). The model described well U(VI) desorption in columns 1 and 2 using the same $K_d = 14$ mL g^{-1} (Figure 1).

The γ-function takes a variety of shapes (*35*, *36*, *39*) that skews toward high rates with increasing η (the shape parameter). Our low values of η (Table 3) indicated that many of the conceptual site/pore groups exhibited small rate constants. We used the same η value for both U(VI) desorption experiments and calculated the value of β (the scale parameter) for each of them. The mean rate constant $\acute{\alpha}$ ($\acute{\alpha} = \eta \times \beta$) for desorption was greater in the fast-flow column

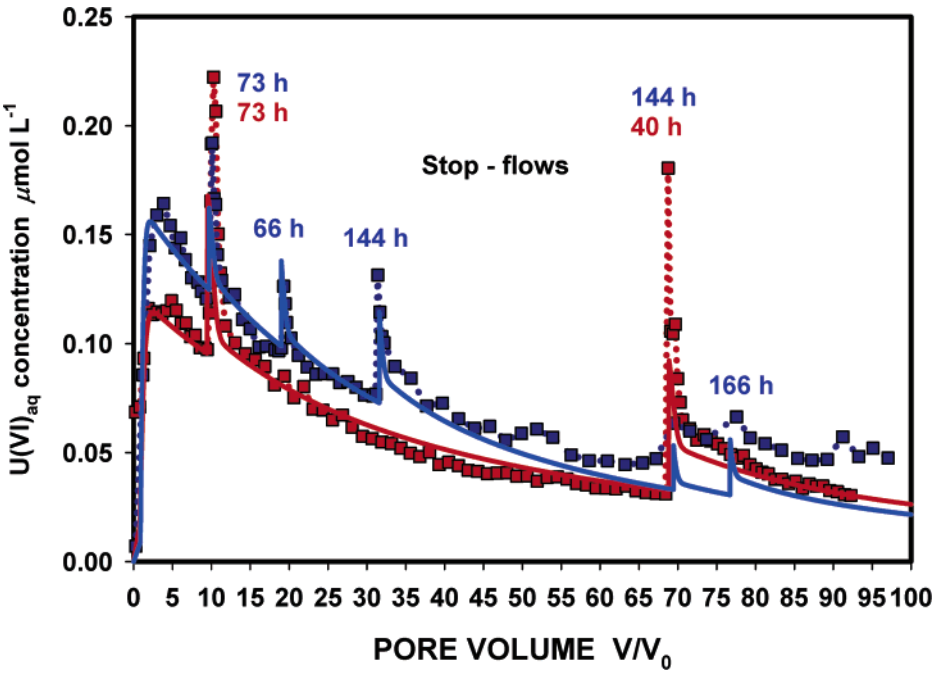

FIGURE 1. Uranium(VI) desorption from contaminated Hanford sediment leached with U(VI)-free SGW [column 1, FRT = 1.1 h (red); column 2, FRT = 9.5 h (blue)]. The model fitted curves are presented with solid lines.

TABLE 3. Parameters[a] Used in Modeling

column ID	K_d (mL g^{-1})	β^b (h^{-1})	η^b	$\acute{\alpha}^b$ (h^{-1})
1 (desorption)	14	0.042	0.42	0.017
2 (desorption)	14	0.011	0.42	0.005
2 (adsorption)	32	0.065	0.22	0.014
3 (adsorption)	22	0.310	0.062	0.019
4 (adsorption)	22	1.30	0.062	0.081
5 (adsorption)	22	0.065	0.22	0.014
6 (adsorption)	22	0.098	0.22	0.022

[a] Other parameters used in modeling were volumetric water content, pore water velocity, and dispersivity. [b] The scale parameter (β), the shape parameter (η), and the mean rate constant ($\acute{\alpha}$).

(Table 3) as expected for a physicochemical process driven by concentration gradient (e.g., diffusion) and/or free energy (e.g., dissolution or release of a surface complex). The U(VI) desorption reaction half-lives varied between 39.3 and 150 h. They were longer than the half-lives of another Hanford sediment (6−63 h; *43*) but were shorter than those of a calcareous soil (~10 yr; *44*).

Unclear for this sediment was the chemical speciation of the aged, sorbed U(VI). Its low total concentration of 22.7 μmol kg^{-1} was well below the sensitivity of spectroscopic methods such as X-ray absorption spectroscopy (XAS; 420 μmol kg^{-1}; e.g., ref *45*) and cryogenic time-resolved laser induced fluorescence spectroscopy (TRLFS; 84 μmol kg^{-1}; e.g., ref *46*). Sorbed U(VI) could exist as surface complex or as a precipitated phase, and the slow desorption rate was consistent with either the diffusion of adsorbed species from lithic fragment or grain coating interiors or the dissolution of a precipitate.

The dynamic waste history and hydrology of this site may have contributed to the partial fixation of U(VI) in the sediment. The pH of the waste infiltration basin that existed approximately 8 m above the capillary fringe sediment varied intermittently from pH 2 to pH 12 during its 32 yr of operation. Transients in subsurface pH may have induced dissolution and precipitation reactions that occluded surface complexes or coprecipitated U(VI). Frequent changes in water content and advective regime over time in response to Columbia River stage variations may have promoted U(VI) redistribution or intragrain transport and may have allowed slow geochemical reactions to yield stable reaction products.

Uranium(VI) Sorption at Low and High Concentrations. To investigate U(VI) sorption in the absence of desorption, a long pulse of SGW with a U(VI) concentration of 0.349 μmol L^{-1} was injected into column 2 after most of the labile U(VI) had been removed (98 PV, Figure 2). The U(VI) BTC exhibited three sections: (i) a long plateau of low and relatively constant U(VI) concentrations (from 98 to 128 PV); (ii) an increasing limb (from 130 to 180 PV) associated with partial breakthrough; and (iii) an upper plateau with $C/C_0 <$ 1 (from 180 to 230 PV). The lack of attainment of C_0 in the upper plateau (iii) indicated that U(VI) sorption was kinetically controlled. The total amount of U(VI) sorbed by the sediment was 5.80 μmol kg^{-1} in 132.5 PV of effluent.

Two additional column experiments were conducted to investigate U(VI) sorption at a higher concentration (~4 μmol L^{-1}; columns 3 and 4; Figure 3). Flow rate or column residence time was again varied (Figure 3a,b). Both columns were leached with the U(VI)-free SGW solution before the injection of U(VI). The transport of U(VI) in these experiments was not affected by contaminant U(VI) desorption because the concentration of the spiked U(VI) was substantially greater than the desorbable U(VI) concentration.

The U(VI) BTCs observed in both columns 3 and 4 were similar to the one observed in column 2 (Figure 3a,b), with the three well-distinguished sections observed previously. The long tailing indicated sorption-related nonequlibrium conditions. The plateau of constant low concentration was shorter, and the increasing limb had a steeper slope in column 4 (Figure 3b, FRT = 1.10 h) than in column 3 (Figure 3a, FRT = 10.21 h). The total amount of sorbed U(VI) was 23.1 μmol kg^{-1} in 58 PV in column 3 and 28.6 μmol kg^{-1} in 80 PV in column 4. Stop flow events in both columns revealed significant nonequilibrium sorption behavior. U(VI) concentrations decreased in all SF events, indicating that the sorption process was kinetically controlled (Figure 3a,b).

A greater K_d (22 mL g^{-1}, Table 3) than the one obtained from fitting desorption experimental data was needed to fit the sorption BTC from columns 3 and 4 (Figure 3). The values

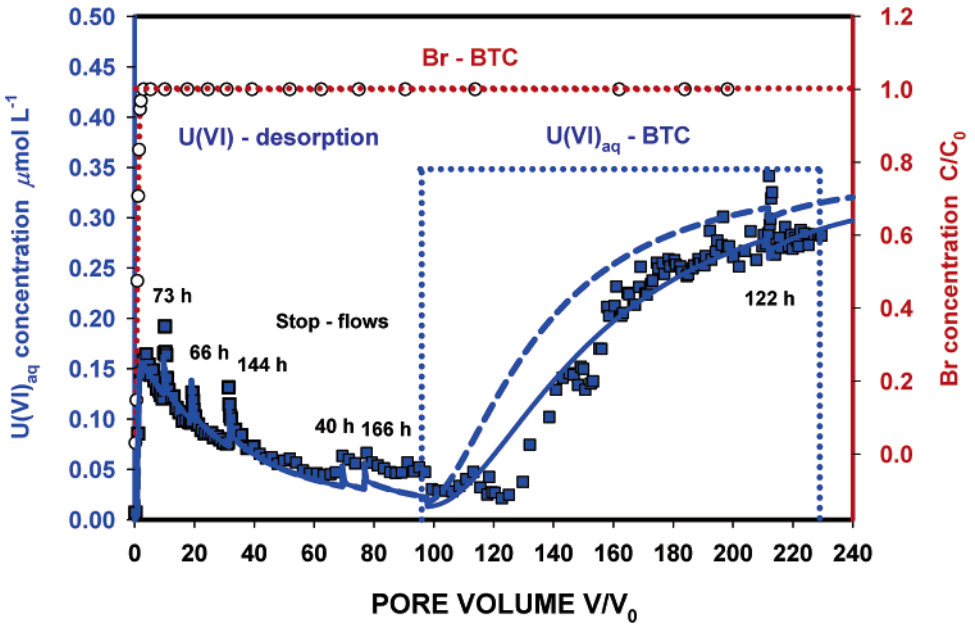

FIGURE 2. BTC for SGW with 0.35 μmol L^{-1} U(VI) after leaching the labile, contaminant U(VI) from the sediment (FRT = 9.5 h). Br BTC is shown with open circles and dotted lines. The effluent pH was 7.99 $\pm$ 0.07 and 7.97 $\pm$ 0.10 during desorption and adsorption, respectively. The model fitted curves are presented with solid (K_d = 32 mL g^{-1}) and dashed lines (K_d = 22 mL g^{-1}).

of R calculated from the fitted K_d values in Table 3 varied between 87 and 127. Retardation decreased with increasing U(VI)(aq) concentration in the injecting solution (compare column 2 with columns 3 and 4, Table 3). The average rate constant calculated with the distributed rate model decreased with increasing FRT during sorption in columns 4 and 3 (from 0.081 to 0.019 h^{-1}).

We assume that adsorption (surface complexation) was the primary sorption process because all U(VI) concentrations in the influent and effluent solutions were computed to be undersaturated with known U(VI) mineral phases. U(VI) may adsorb to the Hanford sediment as a ternary complex with carbonate. U(VI)−carbonate ternary surface species form not only on iron oxides (*3*, *12*, *47*−*51*) but also on hydroxylated edge sites of phyllosilicates (*52*−*55*). Both of these sorbents were present in this sediment.

Like desorption, U(VI) sorption was slow and kinetically controlled, and faster rates were observed in the fast-flow columns. Chemical equilibrium, which for adsorption is usually reached within minutes (*14*), was not attained. Sorption-related nonequlibrium conditions persisted for as long as the experiments were run. One-, two-, three-site, or more complex kinetic models have been used to describe U(VI) sorption kinetics in single (*17*, *56*) or composite mineral materials (*15*, *16*, *18*, *19*, *43*, *44*). We initially tested the equilibrium model and a two-site model that assumed that one group of sites reached equilibrium immediately (equilibrium sites) while the other was kinetically controlled. However, a better fit for both desorption and sorption data was achieved with the distributed rate model. In addition, this model required less fitting parameters then the three- and four-site models. For these reasons, the distributed rate model was therefore selected to describe our experimental data.

The average sorption rates calculated with the γ-distribution model ($\acute{\alpha}$, Table 3) were greater than the desorption rates. The larger β and smaller η values relative to desorption implied that a greater number of site/pore groupings exhibited more rapid rates during sorption, which is to be expected as influent U(VI) sorbs to accessible surface sites that may or may not be the most energetic ones. The elevated values for β at high U(VI) concentration (columns 3 and 4; Table 3) were indicative of increased chemical and/or physical heterogeneity (*36*) (a wider distribution of sites with different rates or diffusional path lengths), which was consistent with the idea that more compartments contributed to the sorption reaction at higher U(VI) concentrations. This "heterogeneity effect" should decrease with increasing FRT, and our modeling results indeed show that the β values are greater at shorter FRTs.

Simultaneous Sorption−Desorption Behavior. To investigate the extent of coupling, or independence of the desorption and sorption reactions, two additional column experiments with different flow regimes (columns 5 and 6) were conducted. These experiments simulate scenarios where U(VI)-enriched recharge waters pass through and react with capillary fringe sediments before discharge to groundwater. Column 5, with a flow regime (FRT) of 9.9 h, was initially leached for 8 PV with the U(VI)-free, SGW solution (Figure 4a). As a consequence, "indigenous" U(VI) was released from the U(VI) labile pool in the contaminated sediment reaching a maximum of 0.178 μmol L^{-1} at 1.8 PV. This concentration was comparable to that in column 2 (Figure 2), which was run at a similar flow rate. Uranium(VI) injected into the column at a concentration of 0.35 μmol L^{-1} beginning at 8 PV exhibited atypical breakthrough (Figure 4a) because of the simultaneous desorption of contaminant U(VI) and sorption of influent U(VI). The total amount of influent U(VI) that was sorbed after 112 PV was 3.82 μmol kg^{-1}, which was smaller than that observed in column 2 (5.80 μmol kg^{-1} after 132.5 PV), indicating interaction between the desorbing and the sorbing U(VI) pools.

The U(VI) effluent concentration was not significantly influenced by SF events at 11 and 38 PV (24 and 48 h, respectively), but it increased markedly (from 0.18 to 0.35 μmol L^{-1}) during the 144 h SF event at 53 PV (Figure 4), indicating that desorption was the controlling kinetic process.

The "go−stop" technique (*57*) was used in column 6 (Figure 4b) to further investigate the coupling of desorption and sorption. The flow rate was adjusted to yield a FRT of 1.1 h for 9−10 h followed by a SF event of 14−16 h. After the addition of influent U(VI) at 13 PV, its effluent concentration increased toward the input value following a similar but more rapid trend than that in column 5. The total amount of U(VI)

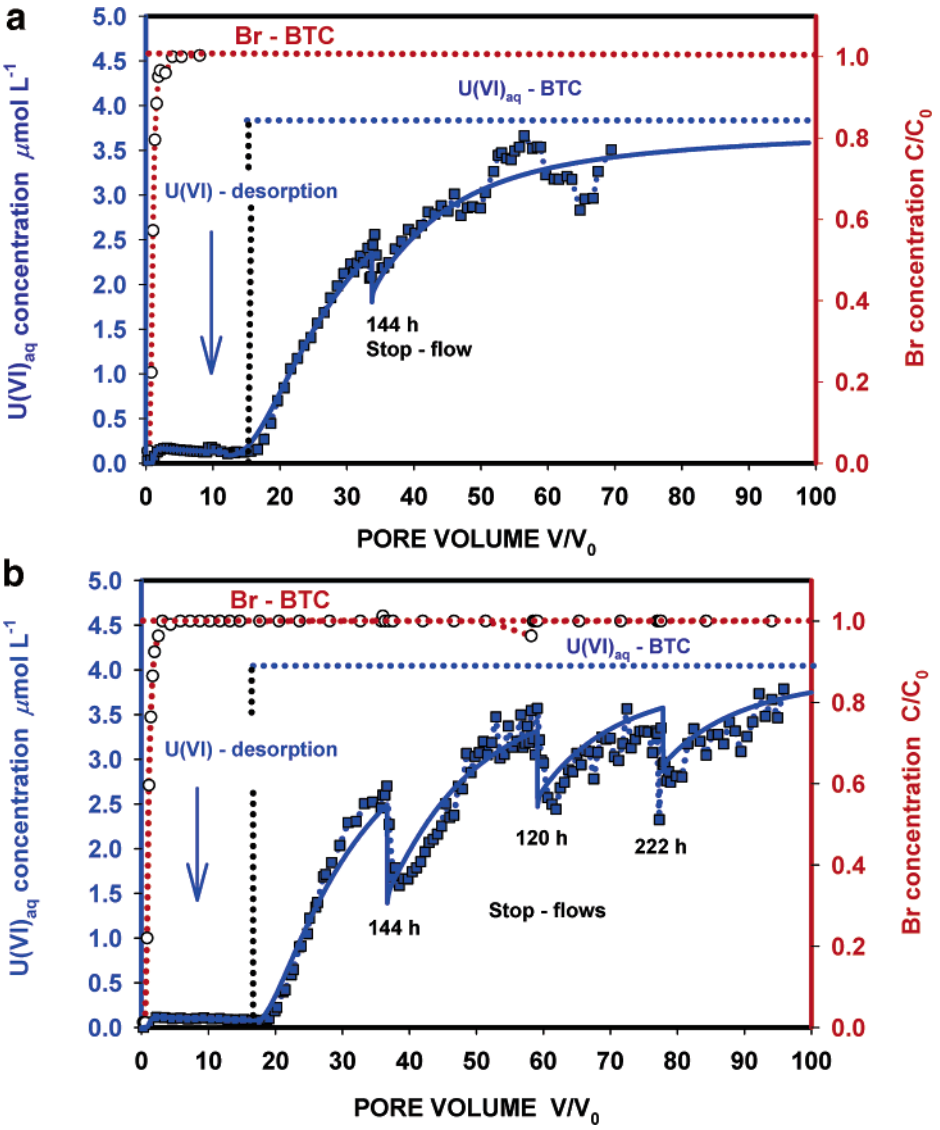

FIGURE 3. BTC for SGW with 4 μmol L^{-1} U(VI) (a: column 3, FRT = 10.21 h; b: column 4, FRT = 1.1 h). Br BTC is shown with open circles and dotted lines. The effluent pH was 7.89 $\pm$ 0.07 and 8.00 $\pm$ 0.05 during desorption and adsorption in column 3 and was 7.94 $\pm$ 0.05 and 7.95 $\pm$ 0.05 during desorption and adsorption in column 4. The model fitted curves are presented with solid lines.

sorbed at experiment termination (2.09 μmol kg^{-1}) was smaller than that in column 5 (3.82 μmol kg^{-1}), indicating that sorption of influent U(VI) was also time-dependent when desorption was occurring simultaneously. Apparently, the short but frequent SF events had no noticeable effect on U(VI) transport since aqueous U(VI) concentrations did not significantly change during these events. The total experimental time in columns 6 and 5 was 257 and 1404 h, respectively.

The K_d values of columns 5 and 6 were considered "apparent K_d values" since the extent of U(VI) sorption was a complex function of U(VI) desorption. The same model parameters used in column 5 (K_d = 22 mL g^{-1}, η = 0.22, and β = 0.065 h^{-1}) were initially used to describe the U(VI) sorption BTC in column 2 after 98 PV (dashed line in Figure 2). However, a better fit was achieved by increasing the K_d from 22 to 32 mL g^{-1} (solid line in Figure 2). It was not resolved whether the best fit K_d in column 2 was higher because of simultaneous desorption in column 5 or because the preleaching of U(VI) in column 2 (0−98 PV) cleared surface sites allowing for more extensive sorption of influent U(VI). Again, the average rate constant decreased with increasing FRT (from 0.022 to 0.014 h^{-1} in columns 6 and 5, respectively).

The average half-life of the U(VI) sorption reaction in all the experiments was 31.3 $\pm$ 16.7 h; a minimum of 8.5 h and a maximum of 48.5 h were observed in columns 4 and 5. These sorption half-lives were relatively long; (*18*, *58*) noted U(VI) sorption half-lives of 25 min and 13.3 h on a goethite-coated sand and Hanford sediment, respectively.

The coupling of the desorption and sorption processes in these experiments produced nontraditional BTCs (Figure 4) that were challenging to decipher. These, however, may represent what occurs in the field as U(VI)-containing vadose zone pore waters or groundwaters interact with the capillary fringe and its low sorbed U(VI) inventory. Close inspection of column 5 results and comparison to those of column 2 (adsorption) that was run at the same flow rate revealed that the breakthrough of influent U(VI) occurred significantly earlier in column 5 than it did during the sorption phase of column 2. Subtraction of the presumed desorption contribution to the column 5 BTC indicated an offset of approximately 10 PV as compared to column 2. This is a conservative estimate as influent U(VI) may suppress desorption through thermodynamic or concentration gradient effects. The offset was also clearly evident in Figure 2a where the best-fit K_d from column 5 predicted early breakthrough

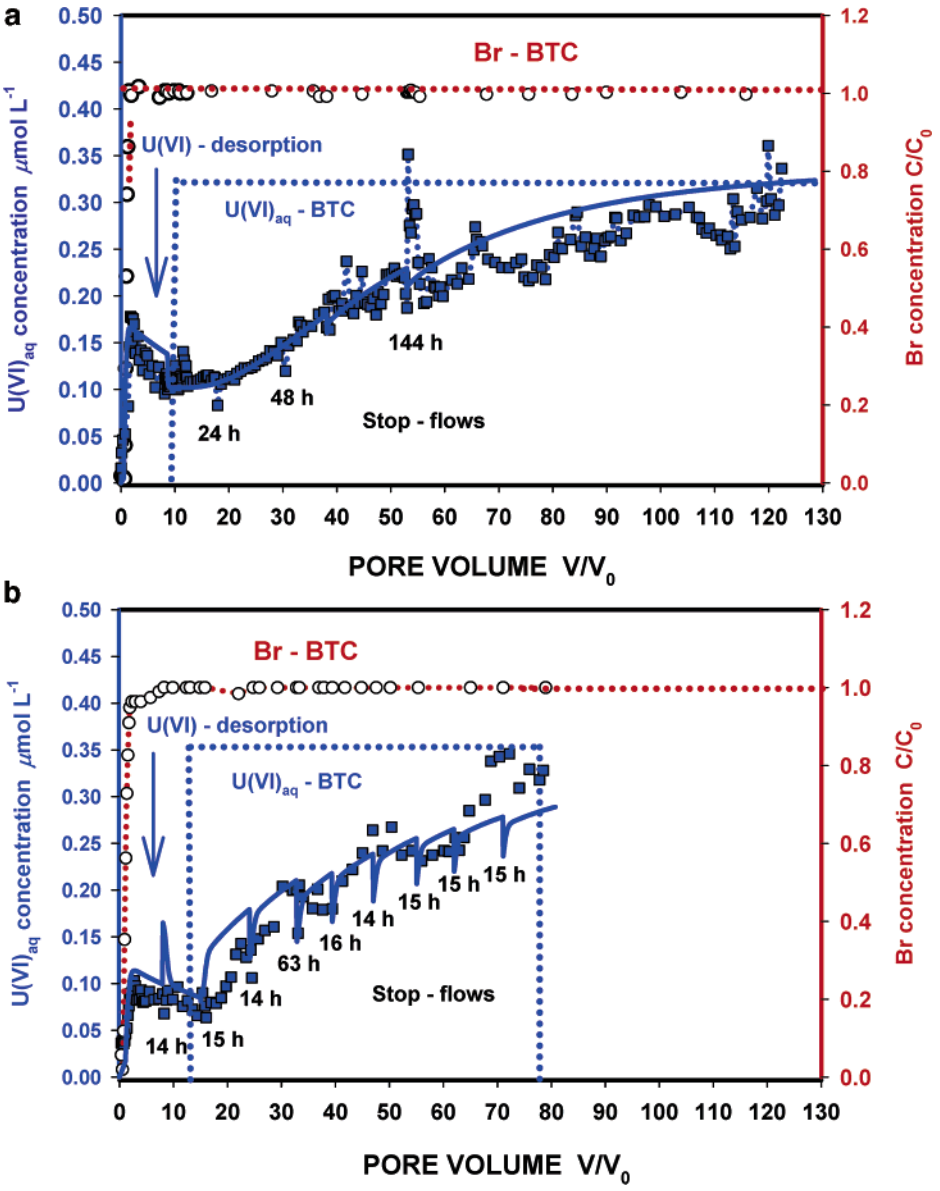

FIGURE 4. BTC for SGW with 0.35 μmol L^{-1} U(VI) (column 5, FRT = 9.9 h; column 6, FRT = 1.1 h). Br BTC is shown with open circles and dotted lines. The effluent pH was 7.96 ± 0.09 and 8.00 ± 0.04 during desorption and adsorption in column 5 and was 7.93 ± 0.13 and 8.06 ± 0.05 during desorption and adsorption in column 6. The model fitted curves are presented with solid lines.

of U(VI) from column 2. Refitting the column 2 data yielded a K_d (32 mL g^{-1}; Table 3) that was markedly higher than column 5 (22 mL g^{-1}).

The preceding observations are consistent with the occurrence of competitive adsorption between the contaminant and influent U(VI) pools. Column 2 results suggested that contaminant U(VI) occupies adsorption sites that may complex influent U(VI) after its removal. It was therefore implied that mass action on a common set of surface complexation sites controlled both desorption and adsorption. Additional research is needed to identify the mineralogical nature of these surface sites and plausible identities for surface complexes.

Conceptual Model. We surmise but cannot yet prove that mass transfer to and from poorly accessible sorbent domains within the sediment fine fraction was responsible for the nonequilibrium sorption−desorption behavior of U(VI). Microscopic evaluation of thin sections of this and other related sediments from the site (by J. P. McKinley, personal communication) showed that sand grains and lithic fragments of various sizes were coated with thin layers of the phyllosilicates that were identified in the fine and clay-sized fractions (e.g., smectite, vermiculite, chlorite). They may represent sorbent domains with limited diffusivity that impact U(VI) sorption rate and extent. We note, however, that our fitting of the two-region, physical nonequilibrium model to the Br BTC implied that all aqueous volume in the columns of sand-textured sediment was mobile. Perhaps the fluid volumes of the poorly accessible domains were too small to influence the macroscopic details of Br BTC or negative charge on the phyllosilicates inhibited inward anion diffusion. In contrast, the neutrally charged, predominant U(VI) species [$Ca_2UO_2(CO_3)_3$(aq)] would have not been excluded from these domains.

Under the oxidizing conditions of this sediment, chlorite, a particularly reactive phyllosilicate, weathers to yield soluble Fe(II) that oxidizes to form poorly crystalline ferrihydrite (*52*, *53*, *59*, *60*), which is a strong U(VI) adsorbent (*34*). Ferrihydrite may have existed in this sediment in both accessible and restricted physical environments before it was collected. Predictions of the sediment U(VI)−K_d using the extractable Fe_{OX} concentration (48 μmol g^{-1}), the diffuse layer com-

plexation model of ref *34*, and a comprehensive suite of aqueous complexation reactions were larger than the observed values in Table 3 supporting the qualitative plausibility of this hypothesis.

Field Implications. The capillary fringe sediment studied here lays at the intersection of a U(VI)-contaminated vadose zone−groundwater system at Hanford. Saturated aquifer materials below the capillary fringe exhibit high hydraulic conductivity and experience the passage of tens of pore volumes of fluid in a given year with pore water velocities comparable to this laboratory study. Variations in river stage cause this capillary fringe material to be part of the vadose zone at low flow (summer/fall) and part of the aquifer system at high flow (winter/spring). The advective desorption studies indicate that contaminated vadose zone materials will function as a long-term source of U(VI) to groundwater. Slow desorption rates combined with low vadose zone water content will likely sustain low-volume, high-concentration U(VI) fluxes to groundwater for the foreseeable future. Groundwaters that are pushed up into the vadose zone will become U(VI) enriched by the same slow desorption process. Enrichment extent will depend on the sorbed U(VI) concentration and the durations of high river stage that regulate contact time. Decreasing river stage and drainage of temporally saturated regions of the lower vadose zone will mobilize U(VI) to groundwater with complex concentration trends exemplified by Figure 4a. Correlations between river stage and groundwater U(VI) concentration are consequently expected and, indeed, observed in monitoring activities (*2*).

Acknowledgments

This research was supported by the U.S. Department of Energy (DOE)—Environmental Management (EM) through the Hanford Remediation and Closure Science Project and the Office of Biological and Environmental Research (OBER) through the EMSP program. Pacific Northwest National Laboratory is operated for the Department of Energy by Battelle. This manuscript benefited greatly from technical reviews of two reviewers and the helpful suggestions made by the Associate Editor, Dr. Janet G. Hering.

Supporting Information Available

Stability constants of U(VI) solid and aqueous species used in speciation modeling, the predominant U(VI) and carbonate species in SGW, Br BTC in columns 1−6, and X-ray diffraction patterns in the clay and fine fractions of the sediment. This material is available free of charge via the Internet at http://pubs.acs.org.

Literature Cited

(1) Riley, R. G.; Zachara, J. M.; Wobber, F. J. *Chemical Contaminants on DOE Lands and Selection of Contaminant Mixtures for Subsurface Science Research*; DOE/ER-0547T; U.S. Department of Energy, Office of Energy Research: Washington, DC, 1992.

(2) Lindberg, J. W.; Peterson, R. E. *300-FF-5 Operable Unit*; Pacific Northwest National Laboratory: Richland, WA, 2004; Chapter 1.12.

(3) Read, D.; Lawless, T. A.; Sims, R. J.; Butter, K. R. Uranium migration through intact sandstone cores. *J. Contam. Hydrol.* **1993**, *13*, 277−289.

(4) Serne, J. N.; Brown, C. F.; Schaef, H. T.; Pierce, E. M.; Lindberg, M. J.; Wang, Z.; Gassman, P. L.; Catalano, J. G. *300 Area Uranium Leach and Adsorption Project*; Pacific Northwest National Laboratory: Richland, WA, 2002.

(5) Kalmykov, S. N.; Choppin, G. R. Mixed $Ca^{2+}/UO_2^{2+}/CO_3^{2-}$ complex formation at different ionic strengths. *Radiochim. Acta* **2000**, *88*, 603−606.

(6) Bernhard, G.; Geipel, G.; Reich, T.; Brendler, V.; Amayri, S.; Nitsche, H. Uranyl(VI) carbonate complex formation: Validation of the $Ca_2UO_2(CO_3)_3$ (aq.) species. *Radiochim. Acta* **2001**, *89*, 511−518.

(7) Clark, D. L.; Hobart, D. E.; Neu, M. P. Actinide carbonate complexes and their importance in actinide environmental chemistry. *Chem. Rev.* **1995**, *95*, 25−48.

(8) Grenthe, I.; Fuger, J.; Konings, R. J. M.; Lemire, R. J.; Muller, A. B.; Nguyen-Trung, C.; Wanner, H. *Chemical Thermodynamics of Uranium*; North-Holland: Amsterdam, 1992.

(9) Tripathi, V. S. Uranium transport modeling: geochemical data and sub-models. Stanford University, 1983.

(10) Hsi, C. D.; Langmuir, D. Adsorption of uranyl onto ferric oxyhydroxides: Application of the surface complexation site-binding model. *Geochim. Cosmochim. Acta* **1985**, *49*, 1931−1941.

(11) Rovira, M.; El Aamrani, F. Z.; Duro, L.; Casas, I.; de Pablo, J.; Brouno, J.; Domenech, C.; Ayora, C. Experimental study and modeling of uranium(VI) transport through ferrous olivine rock columns. *Radiochim. Acta* **2000**, *88*, 6665−6671.

(12) Duff, M. C.; Amrhein, C. Uranium(VI) adsorption on goethite and soil in carbonate solutions. *Soil Sci. Soc. Am. J.* **1996**, *60*, 1393−1400.

(13) Bargar, J. R.; Reitmeyer, R.; Lenhart, J. J.; Davis, J. A. Characterization of U(VI)−carbonate ternary complexes on hematite: EXAFS and electrophoretic mobility measurements. *Geochim. Cosmochim. Acta* **2000**, *64*, 2737−2749.

(14) Giammar, D. E.; Hering, J. G. Time scales for sorption−desorption and surface precipitation of uranyl on goethite. *Environ. Sci. Technol.* **2001**, *35*, 3332−3337.

(15) Baik, M. H.; Cho, W. J.; Han, P. S. Sorption of U(VI) onto granite surfaces: A kinetic approach. *J. Radionanal. Nucl. Chem.* **2004**, *260*, 495−502.

(16) Braithwaite, A.; Richardson, S.; Moyes, L. N.; Livens, F. R.; Bunker, D. J.; Hughes, C. R. Sorption kinetics of uranium-238 and neptunium-237 on glacial sediment. *Czech. J. Phys.* **2000**, *50*, 265−269.

(17) Gabriel, U.; Gaudet, J. P.; Spadini, L.; Charlet, L. Reactive transport of uranyl in a goethite column: an experimental and modelling study. *Chem. Geol.* **1998**, *151*, 107−128.

(18) Gamerdinger, A. P.; Kaplan, D. I.; Wellman, D. M.; Serne, J. N. Two-region flow and rate-limited sorption of uranium(VI) during transport in an unsaturated silt loam. *Water Resour. Res.* **2001**, *37*, 3147−3153.

(19) Gamerdinger, A. P.; Kaplan, D. I.; Wellman, D. M.; Serne, J. N. Two-region flow and decreased sorption of uranium(VI) during transport in Hanford groundwater and unsaturated sands. *Water Resour. Res.* **2001**, *37*, 3155−3162.

(20) Gee, G. W.; Bauder, J. W. Particle size analysis. In *Methods of Soils Analyses. Part 1: Physical and Mineralogical Methods*, 2nd ed.; Klute, A., Ed.; Soil Science Society of America, Inc.: Madison, WI, 1986; pp 383−411.

(21) Mehra, O. P.; Jackson, M. L. Iron oxide removal from soils and clays by a dithionite−citrate system buffered with sodium bicarbonate. *Clays Clay Miner.* **1960**, *7*, 317−327.

(22) Fey, M. V.; LeRoux, J. Properties and quantitative estimation of poorly crystalline components in sesquioxide soil clays. *Clays Clay Miner.* **1997**, *25*, 285−294.

(23) Schwertmann, U. The differentiation of iron oxides in soil by extraction with ammonium oxalate solution. *Z. Pflanzenernaehr. Dueng. Bodenk.* **1964**, *105*, 194−202.

(24) Allison, J. D.; Brown, D. S.; Novo-Gradac, K. J. *MINTEQA2/PRODEFA2, A Geochemical Assessment Model for Environmental Systems: Version 3.0 User's Manual;* U.S. Environmental Protection Agency: Washington, DC, 1991.

(25) Allison, J. D.; Brown, D. S.; Novo-Gradac, K. J. *MINTEQA2/PRODEFA2, A Geochemical Assessment Model for Environmental Systems: User Manual Supplement for Version 4.0*; U.S. Environmental Protection Agency: Washington, DC, 1998.

(26) Qafoku, N. P.; Ainsworth, C. C.; Szecsody, J. E.; Qafoku, O. S. The effect of coupled dissolution and redox reactions on $Cr(VI)_{aq}$ attenuation during transport in the Hanford sediments under hyperalkaline conditions. *Environ. Sci. Technol.* **2003**, *37*, 3640−3646.

(27) Qafoku, N. P.; Ainsworth, C. C.; Szecsody, J. E.; Qafoku, O. S. Transport-controlled kinetics of dissolution and precipitation in the Hanford sediments under hyperalkaline conditions. *Geochim. Cosmochim. Acta* **2004**, *68*, 2981−2995.

(28) Brusseau, M. L.; Hu, Q. H.; Srivastava, R. Using flow interruption to identify factors causing nonideal contaminant transport. *J. Contam. Hydrol.* **1997**, *24*, 205−219.

(29) Parker, J. C.; van Genuchten, M. T. Determining transport parameters from laboratory and field tracer experiments. *Va. Agric. Exp. Stn. Bull.* **1984**, *84*.

(30) Toride, N.; Leij, F. J.; van Genuchten, M. T. *The CXTFIT Code for Estimating Transport Parameters from Laboratory or Field Tracer Experiments*; U.S. Salinity Laboratory: 1999.
(31) Leij, F. J.; Dane, J. H. Moment method applied to solute transport with binary and ternary exchange. *Soil Sci. Soc. Am. J.* **1992**, *56*, 667−674.
(32) Jury, W. A.; Gardner, W. R.; Gardner, W. H. *Soil Physics*; John Wiley & Sons: New York, 1991.
(33) Culver, T. B.; Hallisey, S. P.; Sahoo, D.; Deitsch, J. J.; Smith, J. A. Modeling the desorption of organic contaminants from long-term contaminated soil using distributed mass transfer rates. *Environ. Sci. Technol.* **1997**, *31*, 1581−1588.
(34) Davis, J. A.; Curtis, G. P. *Application of Surface Complexation Modeling to Describe Uranium(VI) Adsorption and Retardation at the Uranium Mill Tailings Site at Naturita, Colorado;* U.S. Nuclear Regulatory Commission: Washington, DC, 2003.
(35) Connaughton, D. F.; Stedinger, J. R.; Lion, L. W.; Shuler, M. L. Description of time-varying desorption kinetics: Release of naphthalene from contaminated soils. *Environ. Sci. Technol.* **1993**, *27*, 2397−2403.
(36) Gustafson, D. I.; Holden, L. R. Nonlinear pesticide dissipation in soils: A new model based on spatial variability. *Environ. Sci. Technol.* **1990**, *24*, 1032−1038.
(37) Lorden, S. W.; Chen, W.; Lion, L. W. Experiments and modeling of the transport of trichloroethen vapor in unsaturated aquifer material. *Environ. Sci. Technol.* **1998**, *32*, 2009−20017.
(38) Chen, W.; Wagenet, R. J. Description of atrazine transport in soil with heterogeneous nonequlibrium sorption. *Soil Sci. Soc. Am. J.* **1997**, *61*, 360−371.
(39) Pignatello, J. J. The measurement and interpretation of sorption and desorption rates for organic compounds in soil media. *Adv. Agron.* **2000**, *69*, 1−73.
(40) Pedit, J. A.; Miller, C. T. Heterogeneous sorption processes in subsurface systems: 1. Model formulation and applications. *Environ. Sci. Technol.* **1994**, *28*, 2094−2104.
(41) Pedit, J. A.; Miller, C. T. Heterogeneous sorption processes in subsurface systems. 2. Diffusion modeling approaches. *Environ. Sci. Technol.* **1995**, *29*, 1766−1772.
(42) Jensen-Spaulding, A.; Cabral, K.; Shuler, M. L.; Lion, L. W. Predicting the rate and extent of cadmium and copper desorption from soils in the presence of bacterial extracellular polymer. *Water Res.* **2004**, *38*, 2230−2239.
(43) Barnett, M. O.; Jardine, P. M.; Brooks, S. C.; Selim, H. M. Adsorption and transport of uranium(VI) in subsurface media. *Soil Sci. Soc. Am. J.* **2000**, *64*, 908−917.
(44) Braithwaite, A.; Livens, F. R.; Richardson, S.; Howe, M. T.; Goulding, K. W. T. Kinetically controlled release of uranium from soils. *Eur. J. Soil Sci.* **1997**, *48*, 661−673.
(45) Catalano, J. G.; Heald, S. M.; Zachara, J. M.; Brown, G. E., Jr. Spectroscopic and diffraction study of uranium speciation in contaminated vadose zone sediments from the Hanford site, Washington State, USA. *Environ. Sci. Technol.* **2004**, *38*, 2822−2828.
(46) Wang, Z.; Zachara, J. M.; McKinley, J. P.; Smith, S. C. Cryogenic laser induced U(VI) fluorescence studies of a U(VI) substituted natural calcite: Implications to U(VI) speciation in contaminated Hanford sediments. *Environ. Sci. Technol.* **2005**, *39*, 0000−0000.
(47) Bargar, J. R.; Reitmeyer, R.; Davis, J. A. Spectroscopic confirmation of uranium(VI)−carbonato adsorption complexes on hematite. *Environ. Sci. Technol.* **1999**, *33*, 2481−2484.
(48) Ho, C. H.; Miller, N. H. Adsorption of uranyl species from bicarbonate solution onto hematite particles. *J. Colloid Interface Sci.* **1986**, *110*, 165−171.
(49) Barnett, M. O.; Jardine, P. M.; Brooks, S. C. U(VI) adsorption to heterogeneous subsurface media: Application of a surface complexation model. *Environ. Sci. Technol.* **2002**, *36*, 937−942.
(50) Payne, T. E.; Harries, J. R. Adsorption of Cs and U(VI) on soils of the Australian arid zone. *Radiochim. Acta* **2000**, *88*, 799−802.
(51) Zheng, Z.; Tokunaga, T. K.; Wan, J. Influence of calcium carbonate on U(VI) sorption to soils. *Environ. Sci. Technol.* **2003**, *37*, 5603−5608.
(52) Pabalan, R. T.; Turner, D. R. Uranium(+6) sorption on montmorillonite: Experimental and surface complexation modeling study. *Aquat. Geochem.* **1997**, *2*, 203−226.
(53) Pabalan, R. T.; Turner, D. R.; Bertetti, F. P.; Prikryl, J. D. Uranium-(VI) sorption onto selected mineral surfaces. In *Adsorption of Metals by Geomedia*; Jenne, E. A., Ed.; Academic Press: San Diego, 1998; pp 99−130.
(54) Payne, T. E.; Lumpkin, G. R.; Waite, T. D. Uranium(VI) adsorption on model minerals. In *Adsorption of Metals by Geomedia*; Jenne, E. A., Ed.; Academic Press: San Diego, 1998; pp 75−99.
(55) Jenne, E. A. Adsorption of metals by geomedia: data analysis, modeling, controlling factors, and related issues. In *Adsorption of Metals by Geomedia*; Jenne, E. A., Ed.; Academic Press: San Diego, 1998; pp 1−73.
(56) Kohler, M.; Curtis, G. P.; Kent, D. B.; Davis, J. A. Experimental investigation and modeling of uranium(VI) transport under variable chemical conditions. *Water Resour. Res.* **1996**, *32*, 3539−3551.
(57) Murali, V.; Aylmore, L. A. G. No-flow equilibration and adsorption dynamics during ionic transport in soils. *Nature (London)* **1980**, *283*, 467−469.
(58) Gabriel, U.; Gaudet, J. P.; Spadini, L.; Charlet, L. Reactive transport of uranyl in a goethite column: an experimental and modeling study. *Chem. Geol.* **1998**, *151*, 107−128.
(59) Arnold, T.; Zorn, T.; Benhard, G.; Nitsche, H. Sorption of uranium(VI) onto phyllite. *Chem. Geol.* **1998**, *151*, 129−141.
(60) Arnold, T.; Zorn, T.; Zanker, H.; Bernhard, G.; Nitsche, H. Sorption behavior of U(VI) on phyllite: experiments and modeling. *J. Contam. Hydrol.* **2001**, *47*, 219−231.

Received for review September 29, 2004. Revised manuscript received February 10, 2005. Accepted February 17, 2005.

ES048462Q